Choosing integration points for QCD calculations by numerical integration

Davison E. Soper
Institute of Theoretical Science, University of Oregon, Eugene, OR 97403
(23 March 2001)

Abstract

I discuss how to sample the space of parton momenta in order to best perform the numerical integrations that lead to a calculation of three jet cross sections and similar observables in electron-positron annihilation.

I. INTRODUCTION

There is an important class of computer programs that do calculations in quantum chromodynamics (QCD) in which the calculation is performed at next-to-leading order in perturbation theory and allows for the determination of a variety of characteristics of the final state. This paper concerns a significant technical issue that arises in such programs when a "completely numerical" integration algorithm is used: how should one choose the integration points?

I consider the calculation of "three-jet-like" observables in e^+e^- annihilation. A given program in the class considered can be used to calculate a jet cross section (with any infrared safe choice of jet definition) or observables like the thrust distribution. Such a program generates random partonic events consisting of three or four final state quarks, antiquarks, and gluons. Each event comes with a calculated weight. A separate routine then calculates the contribution to the desired observable for each event, averaging over the events with their weights.

The weights are treated as probabilities. However, these weights can be both positive or negative. This is an almost inevitable consequence of quantum mechanics. The calculated observable is proportional to the square of a quantum amplitude and is thus positive. However, as soon as one divides the amplitude into pieces for purposes of calculation, one finds that while the square of each piece is positive, the interference terms between different pieces can have either sign. Thus the kind of program discussed here stands in contrast to the tree-level event generators in which, by simplifying the physics, one can generally arrange to have all the weights be positive, or, even, to be all equal to 1.

To understand the algorithms used in the class of programs described above, it is best to think of the programs as performing integrations over momenta in which the quantum matrix elements and the measurement functions form the integrand. There are two basic algorithms for performing the integrations. The older is due to Ellis, Ross, and Terrano (ERT) [1]. (The first general purpose implementation of this method for three-jet-like observables in e^+e^- annihilation was that of Kunszt and Nason [2]). In this method, some of the integrations are performed analytically ahead of time. The other integrations are performed numerically by the Monte Carlo method. The integrations are divergent and are regulated by analytical continuation to $3-2\epsilon$ space dimensions and a scheme of subtractions or cutoffs. The second method is much newer [3,4]. In this method, all of the integrations are done by Monte Carlo numerical integration. With this method, the integrals are all convergent (after removal of the ultraviolet divergences by a straightforward renormalization procedure).

Since this method is quite new, one cannot yet say for what problems it might do better than the now standard ERT method. I can point out that the current incarnation of the numerical method has convergence problems for three jet quantities that receive important contributions from final states that are close to the two jet limit. For example, one gets good results for the three jet cross section or for the thrust distribution away from $T = 1$, but poorly converging results for the energy-energy correlation function. On the other hand, the numerical method offers evident advantages in flexibility to modify the integrand. Thus one should be able to attack problems that are not accessible to the ERT method.

The numerical integration method exists as computer code [5] with accompanying technical notes [6] and many of the basic ideas behind it have been described in the two papers

[3,4]. The present paper is devoted to an exposition of the choice of integration points needed for this method. This subject may seem unimportant. Furthermore, it may seem to be a just a part of the numerical algorithms branch of computer science and thus to be uninteresting from the point of view of physics. However, practitioners of the art of numerical integrations in physics know that the choice of integration points is extremely important. If everything else is perfect but the integration points are badly chosen, the computer will, like Sisyphus, be faced with an unending task because the precision of the answer will not improve as the computational time increases. Furthermore, the problem is a problem in physics. All that the theory of numerical integration tells us is that the density of integration points should be well matched to the structure of the function to be integrated. The function to be integrated comes from Feynman diagrams, so we are really faced with the problem of understanding the structure of the quantum scattering processes. Perhaps surprisingly, the aspects of quantum scattering that are important in numerical method are completely different than the aspects that are important in the ERT method.

In Sec. II below, I briefly review the basics of the numerical integration method with the aim of setting the notation and making it possible to read this paper independently of the previous two papers. Then, in the sections that follow, I turn to the main issue of this paper, the choice of integration points. I try to keep this discussion succinct. The main features of the method are covered, but implementation details are left to the program code and its accompanying technical notes [5,6].

The exposition begins in Sec. III with a review of the general principles of Monte Carlo integration as they apply to this calculation. Sec. IV is the heart of the paper and covers the organization of the method used to choose the most integration points in the most important integration regions. Part of the method used considers the possible three parton final states. This part is explained in Sec. V. The other parts of the method concern the singularities of virtual graphs and their relation to the energy denominators in 2 parton to n parton scattering. The various possibilities are covered in Secs. VI through IX. Of special importance is the elliptical coordinate system introduced in Sec. VI. A brief summary is presented in Sec. X.

II. REVIEW OF THE NUMERICAL METHOD

Let us begin with a precise statement of the problem. We consider an infrared safe three-jet-like observable in $e^+e^- \to \textit{hadrons}$ such as a particular moment of the thrust distribution. The observable can be expanded in powers of α_s/π,

$$\sigma = \sum_n \sigma^{[n]}, \qquad \sigma^{[n]} \propto (\alpha_s/\pi)^n \ . \tag{1}$$

The order α_s^2 contribution has the form

$$\begin{aligned}\sigma^{[2]} = &\frac{1}{2!}\int d\vec{p}_1 d\vec{p}_2 \ \frac{d\sigma_2^{[2]}}{d\vec{p}_1 d\vec{p}_2}\ \mathcal{S}_2(\vec{p}_1,\vec{p}_2) \\ &+\frac{1}{3!}\int d\vec{p}_1 d\vec{p}_2 d\vec{p}_3 \ \frac{d\sigma_3^{[2]}}{d\vec{p}_1 d\vec{p}_2 d\vec{p}_3}\ \mathcal{S}_3(\vec{p}_1,\vec{p}_2,\vec{p}_3)\end{aligned} \tag{2}$$

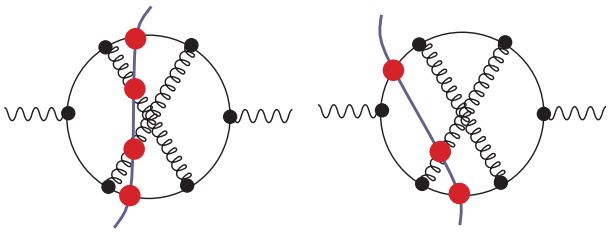

FIG. 1. Two cuts of one of the Feynman diagrams that contribute to $e^+e^- \to$ *hadrons*.

$$+\frac{1}{4!}\int d\vec{p}_1 d\vec{p}_2 d\vec{p}_3 d\vec{p}_4 \; \frac{d\sigma_4^{[2]}}{d\vec{p}_1 d\vec{p}_2 d\vec{p}_3 d\vec{p}_4} \; \mathcal{S}_4(\vec{p}_1, \vec{p}_2, \vec{p}_3, \vec{p}_4).$$

Here the $d\sigma_n^{[2]}$ are the order α_s^2 contributions to the parton level cross section, calculated with zero quark masses. Each contains momentum and energy conserving delta functions. The $d\sigma_n^{[2]}$ include ultraviolet renormalization in the $\overline{\rm MS}$ scheme. The functions $\mathcal{S}$ describe the measurable quantity to be calculated. We wish to calculate a "three-jet-like" quantity. That is, $\mathcal{S}_2 = 0$. The normalization is such that $\mathcal{S}_n = 1$ for $n = 2, 3, 4$ would give the order α_s^2 perturbative contribution the total cross section. There are, of course, infrared divergences associated with Eq. (2). For now, we may simply suppose that an infrared cutoff has been supplied.

The measurement, as specified by the functions $\mathcal{S}_n$, is to be infrared safe, as described in Ref. [7]: the $\mathcal{S}_n$ are smooth functions of the parton momenta and

$$\mathcal{S}_{n+1}(\vec{p}_1, \ldots, \lambda\vec{p}_n, (1-\lambda)\vec{p}_n) = \mathcal{S}_n(\vec{p}_1, \ldots, \vec{p}_n) \tag{3}$$

for $0 \le \lambda < 1$. That is, collinear splittings and soft particles do not affect the measurement.

It is convenient to calculate a quantity that is dimensionless. Let the functions $\mathcal{S}_n$ be dimensionless and eliminate the remaining dimensionality in the problem by dividing by σ_0, the total e^+e^- cross section at the Born level. Let us also remove the factor of $(\alpha_s/\pi)^2$. Thus, we calculate

$$\mathcal{I} = \frac{\sigma^{[2]}}{\sigma_0 \; (\alpha_s/\pi)^2}. \tag{4}$$

Let us now see how to set up the calculation of $\mathcal{I}$ in a convenient form. We note that $\mathcal{I}$ is a function of the c.m. energy $\sqrt{s}$ and the $\overline{\rm MS}$ renormalization scale μ. We will choose μ to be proportional to $\sqrt{s}$: $\mu = A_{UV}\sqrt{s}$. Then $\mathcal{I}$ depends on A. But, because it is dimensionless, it is independent of $\sqrt{s}$. This allows us to write

$$\mathcal{I} = \int_0^\infty d\sqrt{s} \; h(\sqrt{s}) \; \mathcal{I}(A_{UV}, \sqrt{s}), \tag{5}$$

where h is any function with

$$\int_0^\infty d\sqrt{s} \; h(\sqrt{s}) = 1. \tag{6}$$

The quantity $\mathcal{I}$ can be expressed in terms of cut Feynman diagrams, as in Fig. 1. The dots where the parton lines cross the cut represent the function $\mathcal{S}_n(\vec{p}_1, \ldots, \vec{p}_n)$. Each diagram is a three loop diagram, so we have integrations over loop momenta l_1^μ, l_2^μ and l_3^μ. We first perform the energy integrations. For the graphs in which four parton lines cross the cut, there are four mass-shell delta functions $\delta(k_J^2)$. These delta functions eliminate the three energy integrals over l_1^0, l_2^0, and l_3^0 as well as the integral (6) over $\sqrt{s}$. For the graphs in which three parton lines cross the cut, we can eliminate the integration over $\sqrt{s}$ and two of the l_J^0 integrals. One integral over the energy E in the virtual loop remains. We perform this integration by closing the integration contour in the lower half E plane. This gives a sum of terms obtained from the original integrand by some simple algebraic substitutions. Having performed the energy integrations, we are left with an integral of the form

$$\mathcal{I} = \sum_G \int d\vec{l}_1\, d\vec{l}_2\, d\vec{l}_3 \sum_C g(G, C; \vec{l}_1, \vec{l}_2, \vec{l}_3). \tag{7}$$

Here there is a sum over graphs G (of which one is shown in Fig. 1) and there is a sum over the possible cuts C of a given graph. The problem of calculating $\mathcal{I}$ is now set up in a convenient form for calculation.

If we were using the Ellis-Ross-Terrano method, we would put the sum over cuts outside of the integrals in Eq. (7). For those cuts C that have three partons in the final state, there is a virtual loop. We can arrange that one of the loop momenta, say $\vec{l}_1$, goes around this virtual loop. The essence of the ERT method is to perform the integration over the virtual loop momentum analytically ahead of time. The integration is often ultraviolet divergent, but the ultraviolet divergence is easily removed by a renormalization subtraction. The integration is also typically infrared divergent. This divergence is regulated by working in $3 - 2\epsilon$ space dimensions and then taking $\epsilon \to 0$ while dropping the $1/\epsilon^n$ contributions (after proving that they cancel against other contributions). After the $\vec{l}_1$ integration has been performed analytically, the integrations over $\vec{l}_2$ and $\vec{l}_3$ can be performed numerically. For the cuts C that have four partons in the final state, there are also infrared divergences. One uses either a "phase space slicing" or a "subtraction" procedure to get rid of these divergences, cancelling the $1/\epsilon^n$ pieces against the $1/\epsilon^n$ pieces from the virtual graphs. In the end, we are left with an integral $\int d\vec{l}_1\, d\vec{l}_2\, d\vec{l}_3$ in exactly three space dimensions that can be performed numerically.

In the numerical method, we keep the sum over cuts C inside the integrations. We take care of the ultraviolet divergences by simple renormalization subtractions on the integrand. We make certain deformations on the integration contours so as to keep away from poles of the form $1/[E_F - E_I \pm i\epsilon]$, where E_F is the energy of the final state and E_I is the energy of an intermediate state. Then the integrals are all convergent and we calculate them by Monte Carlo numerical integration.

Let us now look at the contour deformation in a little more detail. We denote the momenta $\{\vec{l}_1, \vec{l}_2, \vec{l}_3\}$ collectively by l whenever we do not need a more detailed description. Thus

$$\mathcal{I} = \sum_G \int dl \sum_C g(G, C; l). \tag{8}$$

For cuts C that leave a virtual loop integration, there are singularities in the integrand of the form $E_F - E_I + i\epsilon$ (or $E_F - E_I - i\epsilon$ if the loop is in the complex conjugate amplitude to the right of the cut). Here E_F is the energy of the final state defined by the cut C and E_I is the energy of a possible intermediate state. We will examine the nature of these "scattering singularities" in some detail in the next section. For now, all we need to know is that $E_F - E_I = 0$ on a surface in the space of $\vec{l}_1$ for fixed $\vec{l}_2$ and $\vec{l}_3$ if we pick $\vec{l}_1$ to be the momentum that flows around the virtual loop. These singularities do not create divergences. The Feynman rules provide us with the $i\epsilon$ prescriptions that tell us what to do about the singularities: we should deform the integration contour into the complex $\vec{l}_1$ space so as to keep away from them. Thus we write our integral in the form

$$\mathcal{I} = \sum_G \int dl \ \sum_C \mathcal{J}(G, C; l)\, g(G, C; l + i\kappa(G, C; l)). \tag{9}$$

Here $i\kappa$ is a purely imaginary nine-dimensional vector that we add to the real nine-dimensional vector l to make a complex nine-dimensional vector. The imaginary part κ depends on the real part l, so that when we integrate over l, the complex vector $l + i\kappa$ lies on a surface, the integration contour, that is moved away from the real subspace. When we thus deform the contour, we supply a jacobian $\mathcal{J} = \det(\partial(l + i\kappa)/\partial l)$. (See Ref. [4] for details.)

The amount of deformation κ depends on the graph G and, more significantly, the cut C. For cuts C that leave no virtual loop, each of the momenta $\vec{l}_1$, $\vec{l}_2$, and $\vec{l}_3$ flows through the final state. For practical reasons, we want the final state momenta to be real. Thus we set $\kappa = 0$ for cuts C that leave no virtual loop. On the other hand, when the cut C does leave a virtual loop, we choose a non-zero κ. We must, however, be careful. When $\kappa = 0$ there are singularities in g on certain surfaces that correspond to collinear parton momenta. These singularities cancel between g for one cut C and g for another. This cancellation would be destroyed if, for l approaching the collinear singularity, $\kappa = 0$ for one of these cuts but not for the other. For this reason, we insist that for all cuts C, $\kappa \to 0$ as l approaches one of the collinear singularities. The details can be found in Ref. [4]. All that is important here is that $\kappa \to 0$ quadratically with the distance to a collinear singularity.

Much has been left out in this brief overview, but we should now have enough background to see the requirements for a sensible choice of integration points.

III. GENERAL PRINCIPLES FOR THE CHOICE OF POINTS

In the following sections, we discuss the choice of integration points for the evaluation of a given graph. In this section, we summarize the general principles of Monte Carlo integration as they apply to this calculation.

We wish to perform an integral of the form

$$\mathcal{I} = \sum_G \int dl \ f(G; l) \tag{10}$$

where

$$f(G;l) = \Re\left\{\sum_C \mathcal{J}(G,C;l)\, g(G,C;l+i\kappa(G,C;l))\right\}. \tag{11}$$

(We can take the real part because we know in advance that $\mathcal{I}$ is real.) Using the Monte Carlo technique, for each graph G we choose a large number $\xi(G)N$ of points l, with $\sum_G \xi(G) = 1$ so that the total number of points is N. We sample the points l for graph G at random with a density $\rho(G;l)$, with normalization $\int dl\, \rho(G;l) = 1$. Then the integral is approximated by

$$\mathcal{I}_N = \frac{1}{N}\sum_G \frac{1}{\xi(G)} \sum_{j=1}^{\xi(G)N} \frac{f(l_j)}{\rho(G;l_j)}. \tag{12}$$

This is an approximation for the integral in the sense that, if we repeat the procedure a lot of times, the expectation value for $\mathcal{I}_N$ is

$$\langle \mathcal{I}_N \rangle = \mathcal{I}. \tag{13}$$

The expected r.m.s. error is $\mathcal{E}$, where

$$\mathcal{E}^2 = \langle (\mathcal{I}_N - \mathcal{I})^2 \rangle. \tag{14}$$

With a little manipulation, one can rewrite this as

$$\mathcal{E}^2 = \frac{1}{N}\left\{\sum_G \xi(G)\left[\frac{\Delta(G)}{\xi(G)} - \sum_L \Delta(L)\right]^2 + \left(\sum_L \Delta(L)\right)^2\right\}. \tag{15}$$

where

$$\begin{aligned}\Delta(G)^2 = &\int dl\ \rho(G;l)\left[\frac{|f(G;l)|}{\rho(G;l)} - \int dl'\ |f(G;l')|\right]^2 \\ &+ \int dl\ \Big(|f(G;l)| + f(G;l)\Big) \times \int dl'\ \Big(|f(G;l')| - f(G;l')\Big).\end{aligned} \tag{16}$$

We see, first of all, that the expected error decreases proportionally to $1/\sqrt{N}$. Second, we see that for a given choice of the density functions $\rho(G;l)$, the ideal choice of the factors $\xi(G)$ is $\xi(G) \propto \Delta(G)$. This is, in fact, easy to implement. Third, the ideal choice of $\rho(G;l)$ is $\rho(G;l) \propto |f(G;l)|$. This is, in fact, impossible to implement.

Although it is not possible to choose $\rho(G;l) \propto |f(G;l)|$, at least we can choose it so that $|f(G;l)|/\rho(G;l)$ is not singular at the singularities of $|f(l)|$. Furthermore, we can try to make $\rho(G;l)$ big at places where we know that $|f(G;l)|$ is big.

We will build the general sampling method out of elementary sampling methods. That is, we will find a number of simple methods to choose points l for our graph. Let the density of points for the ith elementary sampling method be $\rho_i(G;l)$ (normalized to $\int dl\, \rho_i(G;l) = 1$). Then we devote a fraction $\lambda_i(G)$ of the points to the choice with density $\rho_i(G;l)$ and obtain a net density

$$\rho(G;l) = \sum_i \lambda_i(G)\, \rho_i(G;l). \tag{17}$$

In this way, we make the sampling problem manageable. If we know that $|f(G;l)|$ is big near a certain point or surface in the space of loop momenta, we can design one of the elementary sampling methods so that the corresponding $\rho_i(G;l)$ is big there. In undertaking this task, we do not have to simultaneously arrange that $\rho_i(G;l)$ be big at other places where $|f(G;l)|$ is big.

In the following sections, we discuss the elementary sampling methods. We imagine that we are dealing with only one specific graph G, so we suppress the index G in the notation.

IV. ORGANIZATION OF THE SAMPLING METHOD

We consider a fixed (uncut) graph, dropping references to the label G of the graph. As mentioned in the previous section, we sample points l in the space of loop momenta according to several elementary sampling methods, each labelled by and index i and having a density of points $\rho_i(l)$. The net density is then $\rho(l) = \sum \lambda_i \rho_i(l)$.

We first address the identification of loop momenta. There are eight propagator momenta $\vec{k}_P$. (See, for example, Fig. 1.) The three loop momenta $\vec{l}_L$ can in general be any three linearly independent linear combinations of the $\vec{k}_P$. We will keep the choice simple by choosing three of the $\vec{k}_P$ to be the loop momenta. However, this still leaves us with the choice of which three of the $\vec{k}_P$ should be loop momenta. It proves convenient to make *different* choices for different elementary sampling methods. We specify the choice by specifying a triplet of integers $\{Q(1), Q(2), Q(3)\}$ such that $\vec{l}_J$ is $\vec{k}_{Q(J)}$. We call Q an index set. Then the complete set of propagator matrices can related to the loop momenta by a matrix A:

$$\vec{k}_P = \sum_{L=1}^{3} A_L^P \vec{l}_L. \tag{18}$$

Evidently, given the index set Q, the matrix A can be constructed by using the topology of the graph.

Now we characterize certain surfaces, to be called scattering singularity surfaces, near which the integrand $|f(l)|$ is big. To do this, we consider the cuts of our graph in which three partons appear in the final state. For each such cut, there is a virtual loop. Let $\vec{l}_1$ be the loop momentum. More precisely, $\vec{l}_1$ will be the momentum, $\vec{k}_{Q(1)}$, of one of the propagators in the loop, but we defer for a moment specifying which one. As specified in Sec. II, the integration contour for $\vec{l}_1$ is deformed into the complex plane,[1] so that $\vec{l}_1 \to \vec{l}_{1,c} = \vec{l}_1 + i\vec{\kappa}$.

Before deformation, the integrand is singular on certain surfaces associated with simple scattering processes, the scattering singularity surfaces. How can this happen? There are four cases. Each case is illustrated by a Feynman graph in Fig. 2. The corresponding scattering singularity surface is illustrated in Fig. 3. The cases are

1. *2 to 2 (s).* A virtual parton with momentum $\vec{l}_1$ merges with a virtual parton with momentum $\vec{l}_2+\vec{l}_3-\vec{l}_1$ to produce a virtual parton with momentum $\vec{l}_2+\vec{l}_3$. This virtual

[1] We keep the momenta that enter the final state real.

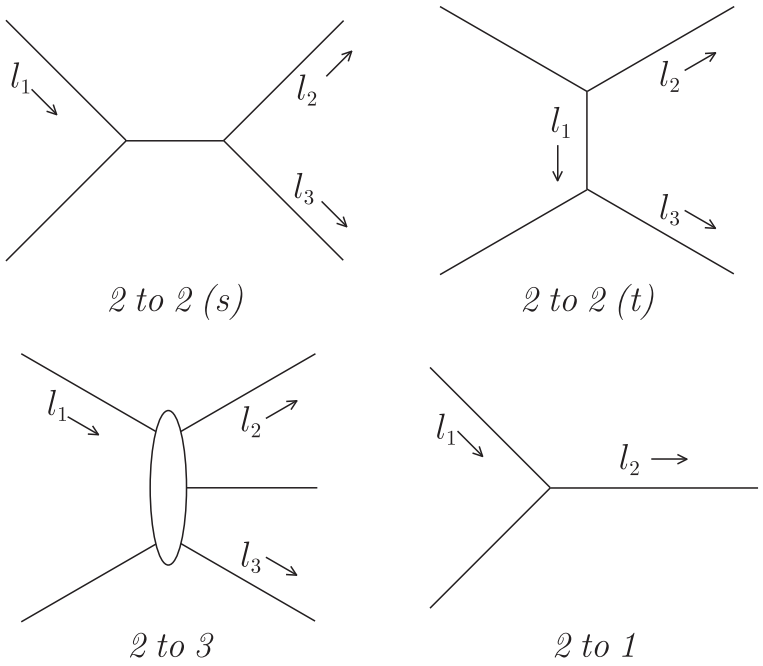

FIG. 2. Elementary scattering subdiagrams that occur at next-to-leading order.

parton divides into two partons with momenta $\vec{l}_2$ and $\vec{l}_3$ that enter the final state. In old-fashioned perturbation theory, there is an energy denominator $|\vec{l}_2| + |\vec{l}_3| - |\vec{l}_1| - |\vec{l}_2 + \vec{l}_3 - \vec{l}_1| + i\epsilon$, which vanishes on the ellipsoid $|\vec{l}_1| + |\vec{l}_2 + \vec{l}_3 - \vec{l}_1| = |\vec{l}_2| + |\vec{l}_3|$ in the space of $\vec{l}_1$. This is the scattering singularity surface. The contour deformation is non-zero on the entire scattering singularity surface.

2. *2 to 2 (t).* A virtual parton with momentum $\vec{l}_2 + \vec{l}_1$ scatters from a virtual parton with momentum $\vec{l}_3 - \vec{l}_1$ by exchanging a parton with momentum $\vec{l}_1$. Partons with momentum $\vec{l}_2$ and $\vec{l}_3$ emerge into the final state. There is a scattering singularity surface $|\vec{l}_2 + \vec{l}_1| + |\vec{l}_3 - \vec{l}_1| = |\vec{l}_2| + |\vec{l}_3|$. In this case, there is also a singularity at $\vec{l}_1 = 0$ that arises from the propagator of the exchanged parton. This soft exchange singularity lies on the scattering singularity surface. Furthermore, in our treatment, the contour deformation vanishes at the soft exchange singularity so that, even after contour deformation, the integrand is singular there. This is, however, an integrable singularity.

3. *2 to 3.* A virtual parton with momentum $\vec{l}_1$ collides with a virtual parton with momentum $-\vec{l}_1$ to produce a final state with partons carrying momenta $\vec{l}_2$, $\vec{l}_3$, and $-\vec{l}_2 - \vec{l}_3$. There is an energy denominator $|\vec{l}_2| + |\vec{l}_3| + |\vec{l}_2 + \vec{l}_3| - 2|\vec{l}_1| + i\epsilon$, which is singular on the sphere $|\vec{l}_1| = [|\vec{l}_2| + |\vec{l}_3| + |\vec{l}_2 + \vec{l}_3|]/2$. The contour deformation is non-zero on the entire scattering singularity surface.

4. *2 to 1.* A virtual parton with momentum $\vec{l}_1$ combines with a virtual parton with momentum $\vec{l}_2 - \vec{l}_1$ to produce an on shell parton with momentum $\vec{l}_2$ that enters the final state. There is an energy denominator $|\vec{l}_2| - |\vec{l}_1| - |\vec{l}_2 - \vec{l}_1| + i\epsilon$, which vanishes on

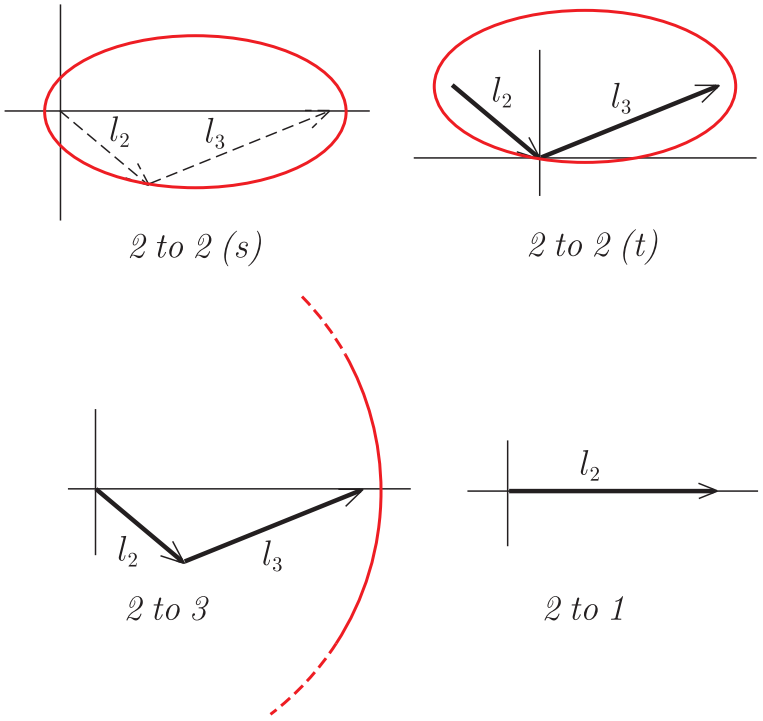

FIG. 3. Singularity surfaces associated with the elementary scatterings in Fig. 2. In each case, the vectors $\vec{l}_2$ and $\vec{l}_3$ (or just $\vec{l}_2$ for *2 to 1* scattering) are indicated by arrows. We see the scattering singularity surface in the space of $\vec{l}_1$. For *2 to 2 (t)* scattering and *2 to 2 (s)* scattering, these surfaces are ellipsoids. For *2 to 3* scattering, the surface is a sphere, only part of which is shown. For *2 to 1* scattering, the surface reduces to a line segment. The integrand is typically not singular on the scattering singularity surface because of the contour deformation. However, the contour deformation vanishes along the heavy straight lines. Thus, in particular, in the *2 to 2 (t)* case the integrand is actually singular at $\vec{l}_1 = 0$.

the line $\vec{l}_1 = x\vec{l}_2$ with $0 \leq x \leq 1$. The contour deformation is chosen to vanish at this collinear singularity. As discussed in Ref. [4], the collinear singularity cancels when one sums over cuts. However, singularities at $\vec{l}_1 = 0$ an $\vec{l}_1 = \vec{l}_2$ remain.

Thus for each cut there are a number of scattering singularity surfaces. There is a contour deformation that keeps the integrand from being singular except at special points on these surfaces. However, the integrand is sometimes still quite large near these surfaces. For this reason, we will design an elementary sampling method for each surface such that the density of points is big on the whole surface and singular at the special point if necessary.

There are two kinds of singularities associated with points $\vec{k}_P = 0$ where a propagator momentum vanishes. First, there is a $1/|\vec{k}_P|^2$ singularity when the momentum of the exchanged parton in a *2 to 2 (t)* scattering vanishes. The elementary sampling method associated with the *2 to 2 (t)* scattering will be designed to take care of this kind of singularity. Second, there is a $1/|\vec{k}_P|$ singularity when *any* propagator momentum $\vec{k}_P$ approaches zero. This weak singularity arises simply because massless Lorentz invariant phase space is $d\vec{k}/|\vec{k}|$. As it turns out, these singularities in the density will automatically be provided by the combined sampling methods without having to specifically arrange for them.

The *2 to 1* scattering singularity surface is exceptional in the list above in that there is no singularity except for the two singular points at $\vec{l}_1 = 0$ and $\vec{l}_2 - \vec{l}_1 = 0$. These two singular points are of one or the other of two types mentioned above. Typically a *2 to 1* scattering subdiagram is part of a *2 to 2 (s)* or *2 to 2 (t)* scattering subdiagram and the two singularities are provided for by the *2 to 2 (s)* or *2 to 2 (t)* sampling methods. The exception is in the case of a self-energy subgraph that is connected to a final state parton. In this case, the *2 to 2 (t)*, *2 to 2 (s)*, and *2 to 3* sampling methods do not apply and we need an explicit *2 to 1* sampling method. Thus we will apply a *2 to 1* sampling method only in the case of a self-energy subgraph connected to a final state parton.

The previous argument indicates that for each scattering singularity surface in the space of the loop momentum $\vec{l}_1$ in a virtual loop, we should associate a method for choosing $\vec{l}_1$ that puts a high density of points near this surface. It is then useful to choose the other two loop momenta to be the momenta of two of the three partons in the final state. Thus the momenta of the final state partons are $\vec{l}_2$, $\vec{l}_3$, and $-\vec{l}_2 - \vec{l}_3$. The integrand will be singular whenever the three partons approach a two jet configuration. Thus we choose the points $\{\vec{l}_2, \vec{l}_3\}$ so that the density of points is appropriately singular at the two jet configurations.

Thus we have a general scheme for organizing the elementary sampling methods. First, find all of the possible three parton cuts of the graph in question. Then, for each such final state cut, enumerate the scattering singularity surfaces that can occur, counting the *2 to 1* case only when the virtual loop is a self-energy diagram connected to a final state parton. There are five basic situations, as illustrated in Fig. 4. Each combination of a final state cut and a scattering singularity surface will correspond to an elementary sampling method.

One point should be emphasized for clarity. In the numerical method discussed in this paper, for each integration point, we compute f/ρ where f is the integrand and ρ is the density of integration points. Contributions from all cuts of a given graph are calculated and summed to form the integrand f. The density ρ is also a sum, with terms corresponding to each of the possible cuts of the graph. Thus there are *independent* sums over possible cuts in f and in ρ.

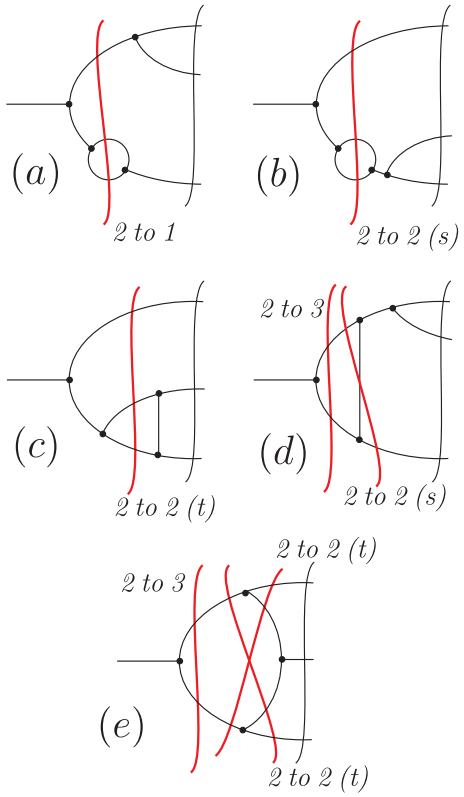

FIG. 4. Matching of scattering singularities to the structure of one loop virtual subdiagrams. A scattering singularity occurs when the energy of an intermediate state matches the energy of the final state. For each diagram, the relevant intermediate states are marked with a line through the graph. The label near the line indicates the type of the corresponding singularity. For some graphs, there is more than one scattering singularity, as indicated. The *2 to 1* singularity is marked only in the case of a self-energy subdiagram connected to a final state parton.

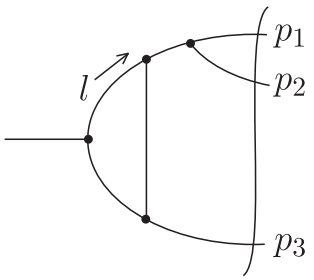

FIG. 5. Labelling of momenta for graphs of type (d) in Fig. 4.

Consider the five basic amplitudes with a virtual loop that are illustrated in Fig. 4. In two of these cases, there are more than one possible intermediate state involving the virtual loop and thus more than one scattering singularity surface. In these cases, it is important to understand how the scattering singularity surfaces fit together.

Let us examine, then, case (d) in Fig. 4. Label the momenta as in Fig. 5. In Fig. 6 we see the scattering singularity surfaces in the space of the loop momentum $\vec{l} \equiv \vec{l}_1$ for an arbitrary fixed choice of the final state momenta $\vec{p}_j$. (We draw the figure for $\vec{l}$ in the plane of the $\vec{p}_j$). The vectors $\vec{p}_1$, $\vec{p}_2$, and $\vec{p}_3$ are indicated. The integration contour is deformed everywhere except along the line $\vec{l} = -x\vec{p}_3$ with $0 < x < 1$, which is indicated as a solid line. There is an ellipsoidal *2 to 2 (s)* surface, $|\vec{l}| + |\vec{p}_1 + \vec{p}_2 - \vec{l}| = |\vec{p}_1| + |\vec{p}_2|$. There is also a spherical *3 to 2* surface, $2|\vec{l}| = |\vec{p}_1| + |\vec{p}_2| + |\vec{p}_3|$. The integration contour is deformed everywhere on both of these surfaces, so that the integrand is not singular anywhere. On the other hand, the deformation vanishes on the solid line, which can be rather near the ellipsoidal surface in the case that the angle between $\vec{p}_1$ and $\vec{p}_2$ is small. Thus the integrand can be rather big on the ellipsoid in this circumstance. Furthermore, the size of the integrand is enhanced where the ellipsoid is tangent to the spherical singularity surface. We will need to put an extra density of points in the region of this point of tangency.

Case (e) in Fig. 4 just a little more complicated. Label the momenta as in Fig. 7. Fig. 6 shows the scattering singularity surfaces in the space of the loop momentum $\vec{l}$ for fixed final state momenta $\vec{p}_j$. The vectors $\vec{p}_1$, $\vec{p}_2$, and $\vec{p}_3$ are indicated. The integration contour is deformed everywhere except along the lines $\vec{l} = x\vec{p}_1$, $\vec{l} - \vec{p}_1 = x\vec{p}_2$ and $\vec{l} - \vec{p}_1 - \vec{p}_2 = x\vec{p}_3$, with $0 < x < 1$ in each case. These lines are are indicated as solid lines that form a triangle. There are two ellipsoidal *2 to 2 (t)* surfaces, $|\vec{l}| + |\vec{p}_1 + \vec{p}_2 - \vec{l}| = |\vec{p}_1| + |\vec{p}_2|$ and $|\vec{l} - \vec{p}_1| + |\vec{l}| = |\vec{p}_2| + |\vec{p}_3|$. There is also a spherical *3 to 2* surface, $2|\vec{l}| = |\vec{p}_1| + |\vec{p}_2| + |\vec{p}_3|$. As in the previous case, (d), we need an especially high density of integration points near where an ellipsoid is tangent to the sphere in the case that this point is near to the triangle, where the deformation vanishes. We have also the new feature that each of the ellipsoids shares a point with the triangle. At this point the contour deformation is zero, so the integrand is actually singular. This is the point where the momentum of the exchanged parton in the associated *2 to 2 (t)* scattering vanishes. The density of integration points will have to have a corresponding singularity at these points.

This completes the description of the general organization of the sampling scheme. In the following sections, we outline its component parts.

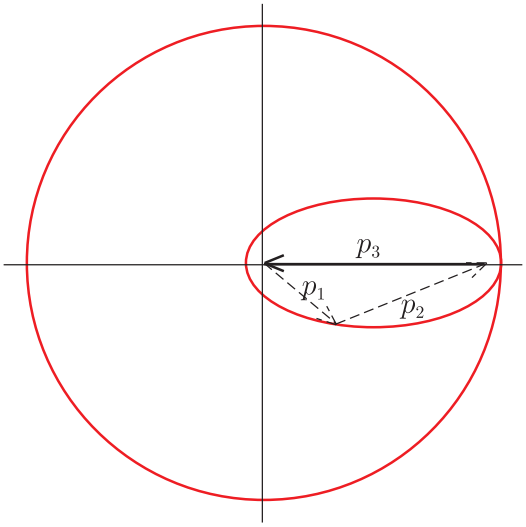

FIG. 6. Singularity surfaces for graphs of type (d) in Fig. 4.

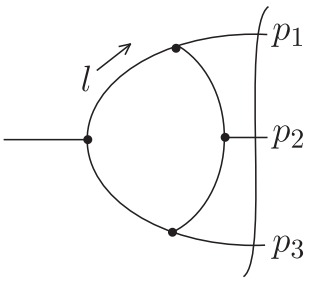

FIG. 7. Labelling of momenta for graphs of type (e) in Fig. 4.

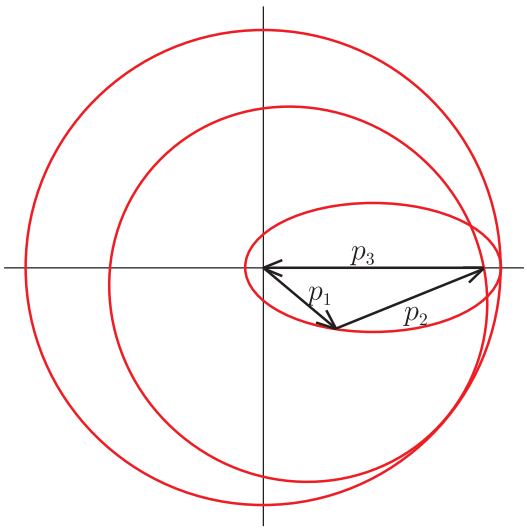

FIG. 8. Singularity surfaces for graphs of type (e) in Fig. 4.

V. SAMPLING FOR THE FINAL STATE

As discussed in the previous section, for each final state cut with three partons in the final state, we will define a number of elementary sampling methods. Part of each method is to choose with an appropriate density the momentum $\vec{l}_1$ that circles through the virtual loop that occurs when there are three final state partons. The other part is to choose the momenta $\vec{l}_2$, $\vec{l}_3$, and $-\vec{l}_2 - \vec{l}_3$ of the final state partons. We address the choice of the final state momenta in this section.

Let the final state parton momenta be $\vec{p}_1$, $\vec{p}_2$, and $\vec{p}_3$, with $\sum_i \vec{p}_i = 0$. (Two of these will then be $\vec{l}_2$ and $\vec{l}_3$, but it doesn't matter which ones.) Define $E_{\max} = \frac{1}{2}\sum_i |\vec{p}_i|$ and $x_i = |\vec{p}_i|/E_{\max}$. Then $\sum_i x_i = 2$ and $0 \le x_i \le 1$. We can write the integration over final state momenta as follows, using $p_3^2 = p_1^2 + p_2^2 + 2p_1p_2\cos\theta_{12}$ so that $d\cos\theta_{12} = p_3 dp_3/(p_1p_2)$:

$$\begin{aligned}\mathcal{I} &= \int d\vec{p}_1\, d\vec{p}_2\, d\vec{p}_3\ \delta(\textstyle\sum \vec{p}_i)\, f(p) \\ &= \int 2E_{\max}^6 d\ln E_{\max}\, d\cos\theta_1\, d\phi_1\, d\phi_{12}\, x_1x_2x_3\, dx_1\, dx_2\, f(p). \end{aligned} \tag{19}$$

Here $\{\theta_1, \phi_1\}$ are the angles of $\vec{p}_1$ and ϕ_{12} is the angle between $\vec{p}_1 \times \vec{p}_2$ and $\vec{p}_1 \times \vec{e}$, where $\vec{e}$ is an arbitrary reference vector.

If we sample $\{\ln E_{\max}, \cos\theta_1, \phi_1, \phi_{12}\}$ with a density

$$\rho_A \equiv \frac{dN}{d\ln E_{\max}\, d\cos\theta_1\, d\phi_1\, d\phi_{12}} \tag{20}$$

and we sample $\{x_1, x_2\}$ with a density

$$\rho_B \equiv \frac{dN}{dx_1\, dx_2}, \tag{21}$$

then the net density is

$$\rho \equiv \frac{dN}{d\vec{p}_1\, d\vec{p}_2} = \frac{\rho_A\rho_B}{2E_{\max}^6\, x_1x_2x_3}. \tag{22}$$

On symmetry grounds, ρ_A should be independent of the angles. Its dependence on $E_{\max}$ is not too important. A convenient choice, normalized so that $\int dN = 1$, is

$$\frac{1}{\rho_A} = \frac{8\pi^2}{3}\,(E_0/E_{\max})^3\left[1 + (E_{\max}/E_0)^3\right]^2, \tag{23}$$

where E_0 is a fixed parameter with dimensions of mass.

What should be the properties of ρ_B? We can expect the integrand $f(p)$ to be singular in any two jet region: when any of the $\vec{p}_j$ vanishes ($x_j \to 0$) or when two of them become collinear (if $\vec{p}_1$ and $\vec{p}_2$ are nearly collinear, then $x_3 \approx 1$). The factor $1/x_1x_2x_3$ in Eq. (22) provides a weak singularity in the $x_i \to 0$ regions. We can build in a weak singularity in the collinear regions by choosing

$$\rho_B = \frac{\mathcal{N}_x\ \max_j \sqrt{1-x_j}}{\prod_j \sqrt{1-x_j}}. \tag{24}$$

The $x_i \to 0$ regions are at the intersections of $x_l \to 1$ regions, so these collinear singularities also enhance the soft singularity of the density. The normalization constant is fixed so that $\int dN = 1$ and is $\mathcal{N}_x = 1/(6\sqrt{2}\arcsin(1/\sqrt{3}))$. One can, of course, change $1/\sqrt{1-x}$ to $1/(1-x)^A$ for any A smaller than 1.

It is a simple matter to actually choose points with the density ρ in Eq. (22). Readers interested in the implementation details may consult the notes [6] that accompany the program code.

I can comment here about the singularities of the integrand, f. If, for the moment, we set the measurement function to 1, then the nominal behavior of f is $f \propto 1/x_j^3$ for $x_j \to 0$ and $f \propto 1/(1-x_j)$ for $x_j \to 1$. This nominal behavior is what one gets after performing the virtual loop integral, $\int dl_1$, inside the $\{\vec{p}_1, \vec{p}_2\}$ integral [8]. These singularities make the integration logarithmically divergent. Then the measurement function that is included in f is required to vanish in the two jet limit, so that the integration becomes convergent. Now, in fact, if we look at the singularities in the $\{\vec{p}_1, \vec{p}_2\}$ integral before performing the virtual loop integral, the singularities are worse than this nominal behavior. For this reason, the suppression of the two jet region coming from the measurement function must be suitably strong in order to obtain good convergence. It remains for future research to arrange the calculation in such a way that the nominal behavior of the integrand f as a function of $\{\vec{p}_1, \vec{p}_2\}$ is obtained.

VI. SAMPLING FOR *2 TO 2 (S)* SCATTERING

In this section, we consider the sampling method associated with *2 to 2 (s)* scattering. We need to choose points $\vec{l} \equiv \vec{l}_1$ appropriate to the following case:

> A virtual parton with momentum $\vec{l}$ merges with a virtual parton with momentum $\vec{l}_2 + \vec{l}_3 - \vec{l}$ to produce a virtual parton with momentum $\vec{l}_2 + \vec{l}_3$. This virtual parton divides into two partons with momenta $\vec{l}_2$ and $\vec{l}_3$ that enter the final state.

In this case, the scattering surface is the ellipsoid $|\vec{l}| + |\vec{l}_2 + \vec{l}_3 - \vec{l}| = |\vec{l}_2| + |\vec{l}_3|$. The density of points should be large on this surface. In order to accomplish this, we use elliptical coordinates.

A. Elliptical coordinates

The elliptical coordinates A_+, A_-, ϕ are defined as follows. First, define κ by

$$2\kappa = |\vec{l}_2 + \vec{l}_3|. \tag{25}$$

Now, define coordinates $A_\pm$ by

$$A_\pm = \frac{1}{2\kappa}\left(|\vec{l}| \pm |\vec{l} - \vec{l}_2 - \vec{l}_3|\right). \tag{26}$$

Then

$$1 < A_+, \qquad -1 < A_- < 1. \tag{27}$$

The coordinate A_+ is constant on elliptical surfaces, while A_- is constant on orthogonal hyperbolic surfaces. The scattering singularity is the ellipsoid

$$A_+ = S_+, \tag{28}$$

where

$$S_\pm = \frac{1}{2\kappa}\left(|\vec{l}_2| \pm |\vec{l}_3|\right). \tag{29}$$

We need one more coordinate. Let ϕ be the azimuthal angle of $\vec{l}$ in a coordinate system in which the z axis lies in the direction of $\vec{l}_2 + \vec{l}_3$ and $\vec{l}_2$ has zero y component and a positive x component. To state this precisely, define unit vectors

$$\begin{aligned} \vec{n}_z &= \frac{\vec{l}_2 + \vec{l}_3}{|\vec{l}_2 + \vec{l}_3|} \\ \vec{n}_y &= \frac{\vec{l}_3 \times \vec{l}_2}{|\vec{l}_3 \times \vec{l}_2|} \\ \vec{n}_x &= \vec{n}_y \times \vec{n}_z. \end{aligned} \tag{30}$$

Then

$$\phi = \arctan\left(\vec{l}\cdot\vec{n}_y / \vec{l}\cdot\vec{n}_x\right). \tag{31}$$

The transformation from A_+, A_-, ϕ to $\vec{l}$ is

$$\vec{l} = \frac{1}{2}(\vec{l}_2 + \vec{l}_3) + l_T\,\cos\phi\;\vec{n}_x + l_T\,\sin\phi\;\vec{n}_y + z\,\vec{n}_z, \tag{32}$$

where

$$\begin{aligned} l_T &= \kappa\left(A_+^2 - 1\right)^{1/2}\left(1 - A_-^2\right)^{1/2} \\ z &= \kappa\, A_+ A_-. \end{aligned} \tag{33}$$

A straightforward calculation shows that the jacobian of the transformation is given by

$$d\vec{l} = \frac{dA_+ dA_- d\phi}{\rho_{AA\phi}}, \tag{34}$$

where

$$\frac{1}{\rho_{AA\phi}} = \kappa^3(A_+^2 - A_-^2). \tag{35}$$

The factor $(A_+^2 - A_-^2)$ is convenient. It provides weak singularities in the density of points when $A_+ \pm A_- \to 0$, which corresponds to $\vec{l} \to 0$ and $\vec{l} - \vec{l}_2 - \vec{l}_3 \to 0$.

If we sample points in the variables $\{A_+, A_-, \phi\}$ with a density

$$\rho' = \frac{dN}{dA_+\, dA_-\, d\phi}, \tag{36}$$

then the total density of points will be

$$\rho = \rho' \times \rho_{AA\phi}, \tag{37}$$

where $\rho_{AA\phi}$ is given in Eq. (35). We next address the question of what to choose for ρ'.

B. The choice of A_+, A_- and ϕ

With what density

$$\rho' = \frac{dN}{dA_+\, dA_-\, d\phi} \tag{38}$$

should we sample points in the variables $\{A_+, A_-, \phi\}$? There is no unique answer, but consider a density function of the form

$$\rho' = \mathcal{N}\, \frac{1}{1 - A_-^2 + \tau}\ \frac{1}{A_+(|A_+ - S_+| + \lambda)}. \tag{39}$$

Here τ and λ are parameters to be specified and the normalization $\mathcal{N}$ is given by

$$\frac{1}{\mathcal{N}} = \frac{2\pi}{\sqrt{1+\tau}}\, \ln\left(\frac{\sqrt{1+\tau}+1}{\sqrt{1+\tau}-1}\right) \left\{\frac{1}{S_+ + \lambda} \ln\left(\frac{S_+[S_+ - 1 + \lambda]}{\lambda}\right) + \frac{1}{S_+ - \lambda} \ln\left(\frac{S_+}{\lambda}\right)\right\}. \tag{40}$$

With this ansatz, there is a high density of points near the scattering singularity surface, $A_+ = S_+$. The width of the peak is λ. Thus λ should be matched to the width of the peak in the integrand. If the singularity surface is far from the line $A_+ = 1$, the contour deformation is substantial and peak is broad. On the other hand, if the singularity surface is near to the line $A_+ = 1$, the contour deformation is small and peak is narrow. I estimate that the width of the peak in the integrand is of order $(S_+ - 1)^2$ for S_+ near 1. For large S_+ it seems reasonable to choose a width of order S_+. Thus I take

$$\lambda = \frac{(S_+ - 1)^2}{S_+}. \tag{41}$$

With the function ρ' in Eq. (39), there is an enhancement of the density of points near $A_- = \pm 1$. This enhancement is built into the density in order to provide an extra density of points near where the ellipsoid in Fig. 6 is tangent to the sphere. As explained in Sec. IV, we need a high density of points here when $\vec{l}_2$ and $\vec{l}_3$ are nearly collinear, that is when S_+ is close to 1. I arrange for this by taking the parameter τ in Eq. (39) to be

$$\tau = \frac{S_+ - 1}{S_+}. \tag{42}$$

It is easy to sample points $\{A_+, A_-, \phi\}$ with the density ρ' in Eq. (39) as explained in [6].

VII. SAMPLING FOR *2 TO 2 (T)* SCATTERING

In this section, we consider the sampling method associated with *2 to 2 (t)* scattering. We need to choose points $\vec{l} \equiv \vec{l}_1$ appropriate to the following case:

> A virtual parton with momentum $\vec{l}_2 + \vec{l}$ scatters from a virtual parton with momentum $\vec{l}_3 - \vec{l}$ by exchanging a parton with momentum $\vec{l}$. Partons with momentum $\vec{l}_2$ and $\vec{l}_3$ emerge into the final state.

In this case, there is a scattering singularity surface $|\vec{l}_2 + \vec{l}| + |\vec{l}_3 - \vec{l}| = |\vec{l}_2| + |\vec{l}_3|$. There is a singularity on this surface at the point where the momentum $\vec{l}$ of the exchanged parton vanishes. The density of points should have a matching singularity at this point.

A. Elliptical coordinates

As in the previous section, we use elliptical coordinates A_+, A_-, ϕ. The role of $\vec{l}$ in the previous section is now played by $\vec{l}+\vec{l}_2$, so the formulas are a little different. We again define κ by $2\kappa = |\vec{l}_2 + \vec{l}_3|$. Now, define coordinates $A_\pm$ by

$$A_\pm = \frac{1}{2\kappa}\left(|\vec{l}_2 + \vec{l}| \pm |\vec{l}_3 - \vec{l}|\right). \tag{43}$$

Then $1 < A_+$ and $-1 < A_- < 1$. Define

$$S_\pm = \frac{1}{2\kappa}\left(|\vec{l}_2| \pm |\vec{l}_3|\right). \tag{44}$$

The scattering singularity is the ellipsoid

$$A_+ = S_+ \tag{45}$$

while the soft exchange singularity is at

$$\{A_+, A_-\} = \{S_+, S_-\}. \tag{46}$$

We need one more coordinate, an azimuthal angle ϕ. We define unit vectors $\{\vec{n}_x, \vec{n}_y, \vec{n}_z\}$ according to Eq. (30). Then we define

$$\phi = \arctan\left((l_2 + \vec{l}) \cdot \vec{n}_y / (l_2 + \vec{l}) \cdot \vec{n}_x\right). \tag{47}$$

The jacobian of the transformation from $\vec{l}$ to $\{A_+, A_-, \phi\}$ is again $1/\rho_{AA\phi}$ where $\rho_{AA\phi}$ is given in Eq. (35). If we sample points in the parameters $\{A_+, A_-, \phi\}$ with a density ρ' then the total density of points will be $\rho = \rho' \times \rho_{AA\phi}$. We next address the question of what to choose for ρ'.

B. The choice of A_+, A_- and ϕ

In this subsection we specify a choice for the density

$$\rho' = \frac{dN}{dA_+\, dA_-\, d\phi} \tag{48}$$

with which we sample in the variables $\{A_+, A_-, \phi\}$. We begin by recognizing that we face two challenges. First, we would like to have a concentration of points near the surface $A_+ = S_+$ with an especially high density near $A_- = \pm 1$ if S_+ is near 1, as discussed with respect to the sampling for *2 to 2 (s)*. The second challenge is to make ρ' appropriately singular at $\{A_+, A_-, \phi\} = \{S_+, S_-, 0\}$. We thus take ρ' to have two parts

$$\rho' = \alpha_{2t}\, \rho_s + (1 - \alpha_{2t})\rho_t, \tag{49}$$

where α_{2t} is a fixed parameter with $0 < \alpha_{2t} < 1$. We take ρ_s to be given by the density (39) for the sampling for *2 to 2 (s)*. Then we have met the first challenge. It remains to design ρ_t to address the second challenge.

The main idea is that there is a scattering singularity surface at $A_+ = S_+$, so that the integrand has a factor

$$\frac{1}{A_+ - S_+ + i\eta} \tag{50}$$

where η is the amount of deformation of the S_+ contour. The amount of contour deformation vanishes at the soft exchange singularity at $\{A_+, A_-, \phi\} = \{S_+, S_-, 0\}$ and, near to this point, η is proportional to the square of the distance to $\{S_+, S_-, 0\}$. Thus, on the surface $A_+ = S_+$ near to the soft exchange singularity, we can estimate η as ω^2 where

$$\omega \equiv |A_- - S_-| + |\phi|/\pi. \tag{51}$$

There is another factor of $1/\omega$ that arises from the propagator of the exchanged parton after we take real-virtual cancellations into account, as explained in detail in Ref. [4]. Thus the absolute value of the integrand has a factor that can be estimated as

$$\frac{1}{\omega |A_+ - S_+|} \tag{52}$$

for $\omega \ll 1$ and $\omega^2 \ll |A_+ - S_+| \ll \omega$. We want ρ_t to have a singularity of the same nature, so that the integrand divided by the density of points is singularity free. Thus we take

$$\rho_t = \frac{\mathcal{A}}{[|A_+ - S_+| + \beta_{2t} S_+ \omega^2][|A_+ - S_+| + \beta_{2t}\gamma_{2t}\, S_+ \omega]}. \tag{53}$$

Here β_{2t} and γ_{2t} are fixed parameters and $\mathcal{A}$ is a rather complicated function of A_- and ϕ (described below) that is of secondary importance. The main point is that ρ_t behaves like (52), with cutoffs when $|A_+ - S_+|$ gets to be smaller than ω^2 or larger than ω.

We have thus given ρ_t an actual singularity at the point $\{A_+, A_-, \phi\} = \{S_+, S_-, 0\}$. This singularity in ρ_t has a special structure such that matches the structure of the integrand f, so that f/ρ_t is finite in the neighborhood of the soft exchange singularity. This point, which is important for the convergence of the numerical integration, was described in some detail in Ref. [4]. In that paper, however, the construction was not as nice as one would like because the ellipsoidal coordinates were not used and the "ridgeline" of ρ was placed on the tangent plane to the ellipsoid rather than on the ellipsoid itself.

To sample points with the density ρ_t of Eq. (53), we sample first in ϕ with a density proportional to $\ln^2(\pi\gamma_{2t}/|\phi|)$. Then, with ϕ chosen, we sample in A_- with a density proportional to $\log(\gamma_{2t}/\omega)/\omega$. Finally, having chosen ϕ and A_-, we sample in A_+ with a density proportional to the right hand side of Eq. (53). Taking into account the normalization conditions, this gives the result in Eq. (53) with

$$\begin{aligned}\frac{1}{\mathcal{A}} = {} & \frac{4\pi}{S_+\beta}\,[\ln^2(\gamma_{2t}) + 2\ln(\gamma_{2t}) + 2]\,\frac{1}{\gamma_{2t} - \omega} \\ & \times \left\{1 + \frac{1}{2\ln(\gamma_{2t}/\omega)} \ln\left(\frac{S_+ - 1 + \beta_{2t} S_+ \omega^2}{S_+ - 1 + \beta_{2t}\gamma_{2t}\, S_+ \omega}\right)\right\} \\ & \times \left\{1 - \frac{1}{2\ln^2(\pi\gamma_{2t}/|\phi|)} \left[\ln^2\left(\frac{\gamma_{2t}}{1 + S_- + |\phi|/\pi}\right) + \ln^2\left(\frac{\gamma_{2t}}{1 - S_- + |\phi|/\pi}\right)\right]\right\}. \end{aligned} \tag{54}$$

The function $\mathcal{A}$ may be a bit complicated, but it is quite benign. In particular, $\mathcal{A}$ is not singular or zero anywhere provided that $\gamma_{2t} > \omega$ holds everywhere. This requires that $\gamma_{2t} > 3$.

VIII. SAMPLING FOR *2 TO 3* SCATTERING

In this section, we consider the sampling method for the third type of scattering singularity surface. We need to choose points $\vec{l} \equiv \vec{l}_1$ appropriate to the following case:

> A virtual parton with momentum $\vec{l}$ collides with a virtual parton with momentum $-\vec{l}$ to produce a final state with partons carrying momenta $\vec{l}_2$, $\vec{l}_3$, and $-\vec{l}_2 - \vec{l}_3$.

In this case, the scattering surface is the sphere $2|\vec{l}| = |\vec{l}_2| + |\vec{l}_3| + |\vec{l}_2 + \vec{l}_3|$. The density of points should be large on this surface. There is no special point embedded in the surface where the density of points needs to be singular. However, the density should be enhanced near the point of this sphere where it intersects the ellipsoid in Fig. 6 or the narrower of the two ellipsoids in Fig. 8.

Since the scattering singularity surface is a sphere, we use spherical polar coordinates $\{r, \cos\theta, \phi\}$ to describe $\vec{l}$. We choose the $\theta = 0$ axis along a certain direction $\vec{P}_C$. In the case (d) illustrated in Fig. 5, we define $\vec{P}_C = -\vec{p}_3$. In the case (e) illustrated in Fig. 7, we define $\vec{P}_C = \vec{p}_1$ if $|\vec{p}_1| > |\vec{p}_3|$ or $\vec{P}_C = -\vec{p}_3$ if $|\vec{p}_3| > |\vec{p}_1|$.

The jacobian of the transformation from $\vec{l}$ to $\{r, \cos\theta, \phi\}$ is

$$d\vec{l} = \frac{dr\, d\cos\theta\, d\phi}{\rho_{r\theta\phi}}, \tag{55}$$

where

$$\rho_{r\theta\phi} = \frac{1}{r^2}. \tag{56}$$

If we sample points in the variables $\{r, \cos\theta, \phi\}$ with a density

$$\rho' = \frac{dN}{dr\, d\cos\theta\, d\phi}, \tag{57}$$

then the total density of points will be

$$\rho = \rho' \times \rho_{r\theta\phi}. \tag{58}$$

We now address the question of how to choose ρ'. Our analysis follows closely that in Sec. VII B. The main idea is that there is a scattering singularity surface at $r = S$, where

$$S = \tfrac{1}{2}\,(|\vec{l}_2| + |\vec{l}_3| + |\vec{l}_2 + \vec{l}_3|). \tag{59}$$

Thus the integrand has a factor

$$\frac{1}{(r/S) - 1 + i\eta}, \tag{60}$$

where η is the amount of deformation of the r/S contour. The amount of contour deformation vanishes quadratically as $\{r, \cos\theta\}$ approaches $\{S_C, 1\}$, where

$$S_C = |\vec{P}_C|. \tag{61}$$

The point $\{S_C, 1\}$ is the point $\vec{l} = \vec{P}_C$. That is, $\vec{l} = -\vec{p}_3$ in Fig. 6 or in Fig. 8 when $|\vec{p}_3| > |\vec{p}_1|$. Thus, on the surface $r = S$, the amount of deformation η can be estimated as Δ^2 where

$$\Delta = \tfrac{1}{3}\sqrt{(1 - S_C/S)^2 + (1 - \cos\theta)}. \tag{62}$$

Thus the absolute value of the integrand has a factor that can be estimated as

$$\frac{1}{|(r/S) - 1|} \tag{63}$$

for $\Delta \ll 1$ and $\Delta^2 \ll |(r/S) - 1| \ll \Delta$. We want ρ' to have a singularity of the same nature, so that the integrand divided by the density of points is singularity free. Furthermore, we would like ρ' to have an extra factor of $1/\Delta^2$ to cancel the factor from the singularity associated with the narrow ellipsoid in Fig. 5 as we approach $\theta = 0$. Thus we take

$$\rho' = \frac{\mathcal{B}}{\Delta\ (|(r/S) - 1| + \alpha_3\Delta^2)\,(|(r/S) - 1| + \alpha_3\Delta)}, \tag{64}$$

where α_3 is a fixed parameter and where $\mathcal{B}$ is a rather complicated but nonsingular function that gets the normalization right:

$$\mathcal{B} = \frac{\alpha_3(1 - \Delta)}{18\pi S}\left[\ln\left(\frac{1}{\Delta^2}\,\frac{1 + \alpha_3\Delta^2}{1 + \alpha_3\Delta}\right)\right]^{-1}\ \left[\ln\left(1 + \frac{2}{(1 - S_C/S)^2}\right)\right]^{-1}. \tag{65}$$

IX. SAMPLING FOR *2 TO 1* SCATTERING

In this section, we consider the sampling method for the fourth type of scattering singularity surface:

> A virtual parton with momentum $\vec{l}$ combines with a virtual parton with momentum $\vec{l}_2 - \vec{l}$ to produce an on shell parton with momentum $\vec{l}_2$ that enters the final state.

As mentioned in Sec. IV, the *2 to 1* scattering singularity surface is exceptional in that there is no singularity except for the two singular points at $\vec{l} = 0$ and $\vec{l}_2 - \vec{l} = 0$. Typically a *2 to 1* scattering subdiagram is part of a *2 to 2 (s)* or *2 to 2 (t)* scattering subdiagram and the two singularities are provided for by the *2 to 2 (s)* or *2 to 2 (t)* sampling methods. The exception is in the case of a self-energy subgraph that is connected to a final state parton. In this case, the *2 to 2 (t)*, *2 to 2 (s)*, and *2 to 3* sampling methods do not apply and we need an explicit *2 to 1* sampling method. Thus we apply a *2 to 1* sampling method only in the case of a self-energy subgraph connected to a final state parton.

We will choose $\vec{l}$ with a density that is a linear combination of five densities:

$$\rho(\vec{l}) = \alpha_{1a}\,\rho_a(\vec{l}) + \alpha_{1b}\,\rho_b(\vec{l}) + \alpha_{1a}\,\rho_a(\vec{l}-\vec{l}_2) + \alpha_{1b}\,\rho_b(\vec{l}-\vec{l}_2) + (1-2\alpha_{1a}-2\alpha_{1b})\,\rho_c(\vec{l}). \quad (66)$$

Here α_{1a} and α_{1b} are fixed positive parameters with $(1-2\alpha_{1a}-2\alpha_{1b})$ also positive.

For $\rho_a(\vec{l})$ we take

$$\rho_a(\vec{l}) = \frac{|\vec{l}_2|}{4\pi}\,\frac{1}{\vec{l}^{\,2}}\frac{1}{\left(|\vec{l}|+|\vec{l}_2|\right)^2}. \quad (67)$$

The density ρ_b is a simple variation on this with $|\vec{l}_2|$ replaced by a scale M:

$$\rho_b(\vec{l}) = \frac{M}{4\pi}\,\frac{1}{\vec{l}^{\,2}}\frac{1}{\left(|\vec{l}|+M\right)^2}. \quad (68)$$

Here $M = (|\vec{l}_2|+|\vec{l}_3|+|\vec{l}_2+\vec{l}_3|)/3$, where the momenta of the particles in the final state are $\vec{l}_2$, $\vec{l}_3$, and $-\vec{l}_2-\vec{l}_3$. The ρ_a and ρ_b terms provide singularities at $\vec{l}^{\,2}=0$ and $(\vec{l}_2-\vec{l})^2=0$.

The ρ_c term provides a non-singular density of points in the neighborhood of the collinear line $\vec{l} = x\vec{l}_2$ with $0<x<1$. For $\rho_c(\vec{l})$ we take

$$\rho_c(\vec{l}) = \frac{\beta_1\gamma_1^2|\vec{l}_2|}{2\pi}\frac{1}{\sqrt{\beta_1^2+(x-1/2)^2}\,\left(\sqrt{\beta_1^2+(x-1/2)^2}+\beta_1\right)\left(\vec{l}_T^{\,2}+\gamma_1^2\vec{l}_2^{\,2}\right)^2}. \quad (69)$$

Here β_1 and γ_1 are fixed parameters and x and $\vec{l}_T$ are defined by writing

$$\vec{l} = x\vec{l}_2 + \vec{l}_T, \quad (70)$$

where $\vec{l}_T$ is the part of $\vec{l}$ that is orthogonal to $\vec{l}_2$.

X. CONCLUSIONS

In a next-to-leading order calculation of three jet cross sections and similar observables in electron-positron annihilation, a given graph leads to several contributions to the cross section. Each of these contributions has the form of a measurement function times a quantum amplitude times a complex conjugate amplitude, as in Fig. 1. We must integrate the sum of these contributions over three loop momenta. In this paper, I have presented a method for sampling the space of loop momenta in order to perform the integrations by the Monte Carlo method.

The main organizing principle for this sampling is to construct the density of integration points as a sum and to have one or more terms in this sum correspond to each possible three parton final state for the graph.

A cut graph with a three parton final state has a virtual loop. We are thus led to consider a simple problem in quantum mechanics: where in the space of the loop momentum are the singularities for two body to n body scatterings? The generic answer is that the singularities

lie on ellipsoidal surfaces. This leads us to choose elliptical/hyperbolic coordinates for the loop momentum space. For the most part, we avoid letting the integrand be truly singular at these surfaces by giving the loop momentum a suitable imaginary part according to the contour deformation recipe of Ref. [4]. Nevertheless, it is helpful to make the density of integration points large near these ellipsoidal surfaces.

We are left with special points on the scattering singularity surfaces where the contour deformation vanishes, so that the integrand is actually singular. This singularity corresponds to soft parton exchange and is significant in gauge field theories. We have seen how to give the density of points a singularity structure that matches that of the integrand as one approaches a soft singularity.

The sampling method that has been described here is far from optimal. It is, however, at least reasonably systematic, and it gives good results for three jet observables that do not get significant contributions from parton final states that are near to two jet configurations.

ACKNOWLEDGMENTS

This work was supported in part by the U.S. Department of Energy.

REFERENCES

[1] R. K. Ellis, D. A. Ross and A. E. Terrano, Nucl. Phys. B **178**, 421 (1981).

[2] Z. Kunszt, P. Nason, G. Marchesini and B. R. Webber in *Z Physics at LEP1*, Vol. 1, edited by B. Altarelli, R. Kleiss ad C. Verzegnassi (CERN, Geneva, 1989), p. 373

[3] D. E. Soper, Phys. Rev. Lett. **81**, 2638 (1998) [hep-ph/9804454].

[4] D. E. Soper, Phys. Rev. D **62**, 014009 (2000) [hep-ph/9910292].

[5] D. E. Soper, *beowulf* Version 1.1, http://zebu.uoregon.edu/∼soper/beowulf/.

[6] D. E. Soper, *Beowulf 1.1 Technical Notes*, http://zebu.uoregon.edu/∼soper/beowulf/.

[7] Z. Kunszt and D. E. Soper, Phys. Rev. D **46**, 192 (1992).

[8] G. Sterman, Phys. Rev. D **17**, 2773 (1978).